

NUMERICAL STUDY TO INVESTIGATE THE EFFECT OF INLET GAS VELOCITY AND REYNOLDS NUMBER ON BUBBLE FORMATION IN A VISCOUS LIQUID

by

**Md. Tariqul ISLAM^a, Poo GANESAN^{a*},
Jaya N. SAHU^b, and Faik A. HAMAD^c**

^a Department of Mechanical Engineering, Faculty of Engineering, University of Malaya, Kuala Lumpur, Malaysia

^b Department of Petroleum and Chemical Engineering, Faculty of Engineering, Institute Technology Brunei, Tungku Gadong, Brunei Darussalam

^c School of Science and Engineering, Teesside University, Middlesbrough, UK

Original scientific paper
DOI: 10.2298/TSC1140825015I

Bubble formation dynamics has great value in mineral recovery and the oil industry. In this paper, a single bubble formation process through an orifice in a rectangle domain is modelled to study the bubble formation characteristics using the volume of fluid with the continuum surface force method. The effect of gas inlet velocities, $U_g \sim 0.1-0.3$ m/s on bubble formation stages (i. e., expansion, elongation, and pinch off), bubble contact angle, dynamics and static pressure, bubble departure diameter etc. was investigated through an orifice diameter of 1 mm. The method was also used to study the effect of Reynolds number, $Re_u \sim 1.32-120$ on bubble formation when all other parameters were kept constant. It is found that a high inlet gas velocity accelerated the reducing of the bubble contact angle from an obtuse angle to an acute angle and the faster development of hemispherical shape of the bubble. It is also found that an increasing of Reynolds number caused speeding up of the bubble pinch-off and formed a smaller bubble neck height due to stronger vortex ring around the bubble neck.

Key words: *volume of fluid, bubble formation, detachment time, Reynolds number*

Introduction

Gas-liquid bubble columns are commonly used as multiphase reactors in chemical, biochemical and environmental engineering, etc., for its advantages such as a high mass and heat transfer and an effective inter-phase contact [1-3]. The bubble formation through orifices is the first process for bubble generation and it is an important process in gas-liquid contacting equipment such as bubble column reactors. Details on the important aspects associated with the bubble formation are given in Kulkarni and Joshi [3]. Some of the factors considered in a series of bubble formation processes are the bubble size, the bubble volume and the frequency of bubble generation and the effect of the preceding bubbles [3, 4]. There have been a number of experimental and analytical studies [5-10] related to bubble formation through a single orifice. For example, Davidson and Schuler [5] experimentally investigated the air bubble formation mech-

* Corresponding author; e-mail: poo_ganesan@um.edu.my

anism through an orifice size of 1.92 mm in liquids of high viscosities ranging from 0.5 to 1.04 Pa·s for both constant gas flow and constant gas pressure conditions. The air was supplied at flow rates ranging from 0 to 50 ml/s (or inlet velocity from 0 to 17.26 m/s). They found that the bubble volume depends on constant gas flow rate. But for constant gas pressure condition, the bubble volume depended on the orifice diameter. Badam *et al.* [10] investigated the bubble formation using a submerged orifice under water and propanol solution for a wide range of gas flow rates (*i. e.*, 75 to 3000 cm³/min). The effects of orifice diameters (*i. e.*, 2, 4 and 6 mm) and surface tension on the bubble formation were studied. They have found that, the volume of bubble or the bubble formation time increased with increase in orifice diameter and higher surface tension. Similarly, Valencia *et al.* [11] utilized the volume-of-fluid (VOF) numerical method to investigate the bubble formation, the rise velocity and the bubble interaction with the free surface using inlet gas velocity of 0.2 m/s passing through 2.5 mm orifice diameter. The authors found that the formation of the first bubble required a longer period than that of the following second bubble. Gerlach *et al.* [12] and Chakraborty *et al.* [13] used the coupled level set and VOF method to investigate the bubble formation dynamics. Gerlach *et al.* [12] investigated the effect of the liquid properties and operating conditions on bubble formation and the detachment bubble from 2 mm orifice diameter at a constant air flow rate of 100 ml/min. They found that the bubble size (or volume) increases with the decrease of the liquid density as well as with the increase of the viscosity and the surface tension coefficient. Chakraborty *et al.* [13] investigated the effect of reduced gravitational forces (*i. e.*, 0.98 - 0.098 m/s²) on bubble formation for a constant air flow rate in the range of 0.167·10⁻⁶ to 3.33·10⁻⁶ m³/s is supplied through an orifice diameter of 3 mm. They have found that the detached bubble size (or volume) increases, but the bubble formation frequency decreases with the decrease of the gravitational force.

In the present study, the VOF method with the continuum surface tension force (CSF) model have been used to investigate the bubble formation dynamics in viscous fluid. The CSF model has been incorporated into the momentum equation as a source term [14]. In VOF, the piecewise linear interface calculation (PLIC) was used to overcome the numerical diffusion problem [15]. In summary, various experimental and numerical studies on a single bubble formation in bubble columns as given above, but the detailed information of a bubble formation from an orifice such as the bubble formation stages, bubble contact angle and pressure, *etc.* in the bubble column are not available. The objective of this study is to investigate the effect of the inlet gas velocity on bubble formation stages (*i. e.*, expansion, elongation, and detachment); bubble contact angle, dynamics pressure, static pressure and bubble equivalent diameter using VOF-CSF model. Three gas velocities of 0.1, 0.2, and 0.3 m/s were used to supply the air through an orifice of 1 mm diameter into the glycerine solution. The model was also used to study the effect of Reynolds number (Re_{μ}) on bubble formation dynamics. For this study, a wide range of Re_{μ} from 1.32 to 120 was considered when the parameters were kept constant. The model was validated by comparing bubble rise velocity and the shape of bubble during formation stages with some experimental data from the literature [5, 16, 17], before reporting the findings.

Mathematical model

Governing equations

The VOF method is used to numerically investigate the motion of the bubble, which is based on Navier-Stokes equations and it is solved for a mixture phase system [18]. The continuity equation and momentum equation are:

$$\nabla \vec{V} = 0 \quad (1)$$

$$\frac{\partial}{\partial t}(\rho \vec{V}) + \nabla(\rho \vec{V} \vec{V}) = -\nabla P + \nabla[\mu\{\nabla \vec{V} + (\nabla \vec{V})^T\}] + \rho \vec{g} + \vec{F} \quad (2)$$

where, \vec{V}, ρ, μ, P, t , and $\vec{g} = (0, -g)$ is the velocity vector, the density of the fluid, the viscosity of the fluid, the pressure, the time, and the gravitational acceleration, respectively. A continuity equation is solved for the volume fraction of gas phase to track the gas-liquid interface:

$$\frac{\partial}{\partial t}(\alpha_g) + \vec{V} \nabla \alpha_g = 0 \quad (3)$$

So the volume fraction of liquid phase is computed by the equation:

$$\alpha_l + \alpha_g = 1 \quad (4)$$

where α_g and α_l is the volume fraction of gas and liquid phase, respectively. Phases' property data are used in the transport equations and also to determine the gas and liquid phase component in each control volume. The density and viscosity of the mixed fluid at interface in each cell are computed by the equations:

$$\rho = \rho_l \alpha_g + \rho_g [1 - \alpha_g] \quad (5)$$

$$\mu = \mu_l \alpha_g + \mu_g [1 - \alpha_g] \quad (6)$$

where ρ_g, ρ_l, μ_g , and μ_l is the density and the viscosity of the gas and the liquid phase, respectively.

Continuum surface tension equation

The dynamic stress balance is realized through the CSF equation, which is incorporated in the momentum equation by introducing a volume force, \vec{F} as described by Brackbill *et al.* [14]. This localized volume force is calculated from the volume fraction data using the equation:

$$\vec{F} = \frac{2\sigma k \nabla \alpha_l}{\rho_g + \rho_l} \quad (7)$$

where k is the surface curvature of the interface which is defined in terms of divergence of the unit vector, \hat{n} , and it is calculated by using the equation:

$$k = (\nabla \hat{n}) = \frac{1}{|\hat{n}|} \left[\left(\frac{\vec{n}}{|\vec{n}|} \nabla \right) \cdot \hat{n} - (\nabla \hat{n}) \right] \quad (8)$$

where $\hat{n} = \vec{n}/|\vec{n}|$.

The PLIC method [15] is used to the gas and liquid interface in Fluent [19].

Computational domain, boundary conditions and numerical procedure

A 2-D rectangle domain with 100 mm height and 50 mm width as shown in fig. 1(a) is used to represent the formation of a single bubble in a column. The effect of side wall to the bubble is neglected because the small ratio of the bubble size to the column width [20]. An orifice for the gas inlet is located at the bottom wall of the column, which is assigned as 'velocity inlet' boundary condition (BC). The top wall is assigned as pressure outlet BC. The side walls are assigned as no slip BC. The operating pressure is set to be equal to the ambient pressure, *i. e.*,

101325 Pa and the gravitational force (g) of -9.81 m/s^2 is assigned along y -axis. Three different inlet gas velocities of 0.1 m/s, 0.2 m/s, and 0.3 m/s are supplied through the constant orifice diameter of 1 mm. The varying inlet gas velocities are selected based on that which is used in industrial bubble columns, [21, 22]. Air is fed into the glycerine solution through the orifices and the bubble formation process and the bubble shape are investigated numerically.

Ansys-Fluent CFD software [19] which is based on the finite volume method is used to solve the governing equations. To minimize the numerical diffusion, the QUICK scheme is applied to solve the momentum equation. The pressure implicit with splitting operators (PISO) algorithm is used in the pressure-velocity coupling. Pressure is solved using a PRESTO scheme. The transient model is based on an explicit scheme in Fluent and Courant number is set to 0.25 corresponding to a time step of 0.0001 s. Under relaxation factor of 0.3 and 0.7 is set for the pressure and momentum, respectively, to assist convergence. The scaled residuals of $1 \cdot 10^{-6}$ are set as the convergence criteria for all the governing equations.

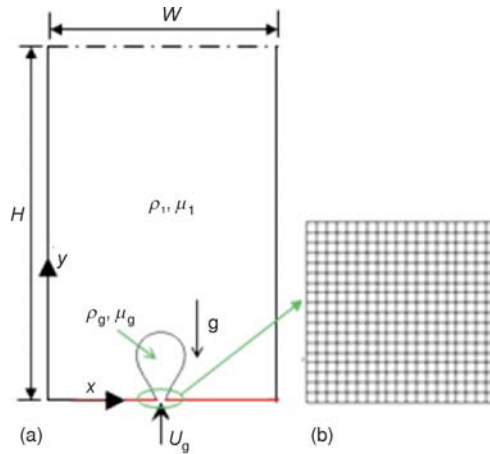


Figure 1. (a) Computational domain of gas-liquid bubble column (b) zoom view of uniform structured grid near the orifice mouth.

Grid dependency test

A uniform structured grid of $0.25 \text{ mm} \times 0.25 \text{ mm}$ is used everywhere in the domain. Figure 1(b) shows the magnified view of the mesh used near the orifice of the domain. The effect of mesh sizes on results is investigated using three types of meshes, *i. e.*, $0.20 \text{ mm} \times 0.20 \text{ mm}$, $0.25 \text{ mm} \times 0.25 \text{ mm}$, and $0.30 \text{ mm} \times 0.30 \text{ mm}$, resulting in a total number of elements of 126252, 80000, and 56112, respectively. For the grid study, the bubble aspect ratio is investigated under the simulation condition of 0.1 m/s inlet gas velocity through a 1 mm orifice diameter. The aspect ratio is given as the ratio of the bubble height to width. Figure 2 shows the aspect ratio with the increase in the simulation time for the three types of meshes. Note that these results were taken after the bubble had detached itself from the orifice. The results from the three types of meshes show a slight difference in that for the $0.25 \text{ mm} \times 0.25 \text{ mm}$ mesh, the difference is even smaller. For this reason, the mesh with $0.25 \text{ mm} \times 0.25 \text{ mm}$ dimensions is selected for the current study to comprise accuracy and the computation cost.

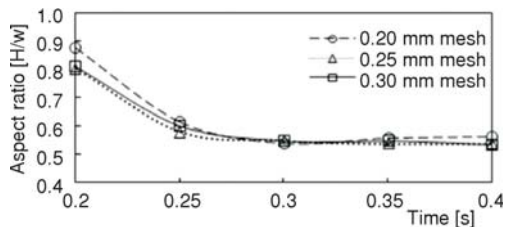


Figure 2. Bubble aspect ratio as a function of time at different size of meshes

Simulation cases

A total of 15 simulation cases were carried out. A summary of all the simulation cases is given in tab. 1. The first four cases were used for validation in which two different diameter of 4 mm and 5 mm are set to rise in stagnant water (cases 1-2); glycerine solution (cases 3-4) from a

rest condition and from an initial position of 10 mm vertical height of the domain. Zero velocity is set at the orifice inlet BC. This also means that the orifice is treated as a wall for these validation cases.

Table 1. Simulation cases

Case	ρ_1 [kgm ⁻³]	μ_1 [Pa·s]	d_o [mm]	Re_μ	Bo_b	Inlet BC U_g [ms ⁻¹]	Purpose
1-2 3-4	1000 1205	0.007 0.076	0	127-154 9.4-12.7	2.8-3.4 3-4.7	0	Validation with experimental data [16, 17]
5-7	1205	0.076	1	1.58 3.17 4.76	0.187	0.1 0.2 0.3	To investigate the effect of inlet gas velocity on the bubble formation mechanism
8-11	1205	0.076 0.050 0.025 0.001	1	1.58 2.41 4.82 120	0.187	0.1	To investigate the effect of Reynolds number on the bubble formation mechanism
12-15	1000	0.076 0.050 0.025 0.001	1	1.32 2.00 4.00 100	0.156	0.1	To reduce the density to be the same as that of water

Three cases (cases 5-7) have been used to investigate the effect of inlet gas velocity (*i. e.*, 0.1 m/s, 0.2 m/s, and 0.3 m/s) through an orifice diameter, $d_o = 1$ mm on the bubble formation. Four cases (cases 8-11) are used to investigate the effect of Reynolds number in range of 1.58-120, which are varied using the liquid viscosity and density value, using $U_g = 0.1$ m/s and $d_o = 1$ mm. The last four cases (cases 12-15) are similar to cases 8-11 but the density of the liquid is reduced to be the same as that of water. Glycerine solution (82% glycerine and 18% water) is used as the liquid phase and air is used as the gaseous phase. The material properties of the liquid density, $\rho_1 = 1205$ kg/m³, viscosity, $\mu_1 = 0.076$ Pa·s, and surface tension, $\sigma = 0.063$ N/m are taken from Raymond and Rosant [17].

Results and discussion

Model validation

The present simulation results are compared with numerical and experimental results from the available literature. Two types of liquid medium (*i. e.*, water and glycerine solution) are used in the column for the validation purpose. A 4 mm and 5 mm bubble diameter are set to rise from a rest condition and from an initial position of 10 mm vertical height of the domain. Zero velocity is set at the orifice inlet BC. It means that the orifice is treated as a wall for this validation cases. The bubble moved up under the action of the buoyancy force and the bubble terminal velocity has been considered after the less fluctuation of instantaneous rise velocity of the bubble. Additionally, the bubble terminal velocity calculated using Krishna *et al.* [23] correlation which was developed for air-water system: $U_T = SF [(2\sigma/\rho_1 d_b) + (gd_b/2)]^{0.5}$; $SF = [1 - (d_b/D_c)]^{1.5}$. Where SF , D_c , and d_b is the scale factor, the column diameter, and the bubble diameter, respectively. The terminal velocity of 4 mm and 5 mm bubble diameter is 0.2345 m/s and 0.2283 m/s, respectively. All the results are summarized in tab. 2, which shows the comparison of the terminal velocity from the simulation, theoretical calculation using Krishna *et al.* [23] correlation and that from experimental

investigation of Krishna and Van Baten [16] in water and Raymond and Rosant [17] in glycerine solution. The deviation of the terminal velocities from the simulation is less than 6% in comparison with the literature data. Therefore, these comparisons provide a good benchmark for the present simulation model in the current study.

Table 2. Comparison of the bubble terminal velocity from present simulation, theoretical calculation using Krishna *et al.* [23] correlation and that from experimental investigation of Krishna and Van Baten [16] in water; Raymond and Rosant [17] in glycerine solution

Primary phase	Bubble diameter, d_b [mm]	Simulation result [ms^{-1}]	Correlation result [ms^{-1}]	Experimental result [ms^{-1}]	Relative error [%]
Air-water	4	0.225	0.233 [23]	0.239 [16]	5.84
	5	0.218	0.227 [23]	0.231 [16]	5.62
Air-glycerine	4	0.144	–	0.145 [17]	0.7
	5	0.156	–	0.164 [17]	4.87

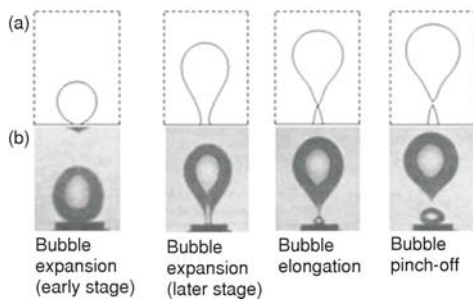


Figure 3. (a) Computed bubble shape from the simulation and (b) experiment bubble shape from Davidson and Schuler [5] at orifice diameter of 1 mm and $U_g = 0.2$ m/s

Another validation study using an orifice diameter of 1 mm and inlet gas velocity of 0.2 m/s at the orifice, our numerically computed bubble and its shape near the orifice in a glycerine solution is compared with that from experimental investigation of Davidson and Schuler [5]. Figure 3(a) and 3(b) show bubble's expansions, elongations and detachment stages at the orifice from the simulation and the experiment. This comparison shows a good agreement and indicates that the present CFD model is capable to predict accurate results for the investigation of single bubble characteristics in a bubble column.

Numerical bubble formation mechanism

The bubble formation is considered to take place in two stages. The first stage results in the formation of a near spherical bubble which continues to grow until force balance, when the upward forces (buoyancy force and momentum force), are in balance with the downward forces (surface tension force, drag force, and inertia force). The second stage (bubble growth after force balance) starts when the upward forces are greater than the downward forces and the bubble starts to move away from the nozzle. The bubble will not lose its contact with the nozzle during this stage and the dispersed phase will continue to flow into the bubble and its detachment tail. During the second stage, the bubble volume increases and the bubble accelerate until the pinch-off from the nozzle, when the bubble has moved a distance of $0.5d_0 + 2.0$ for liquid bubbles [8]. However, this distance is different for a gas bubble which is more than twice the orifice diameter as reported by Kim *et al.* [24].

Figures 3(a) and 3(b) also represent the different stages of the bubble formation. The bubble growth during the early stages where it attaches to the mouth of the orifice, results in the formation of a near spherical shape (early stage of expansion) to a slender neck shape (later stage

of expansion). In the elongation stage, the neck of the bubble near the orifice grows longer and slender due to the constant inlet gas flow but the neck still connects to the orifice. In detachment stage, the slender neck pinches off and the bubble detaches from the orifice mouth. It is clear that the present simulation is able to show the mechanism of bubble formation and generation from the orifice. The simulation results showed that the bubble pinches off from the orifice when the length of the slender neck (*i. e.*, 2.23 mm) is greater than the orifice diameter (*i. e.*, 1 mm) and this is consistent with that reported by Kim *et al.* [24].

Effect of inlet gas velocity on bubble formation

The effect of inlet gas velocity (*i. e.*, 0.1 m/s, 0.2 m/s, and 0.3 m/s) on the bubble formation is investigated using an orifice diameter of 1 mm and the formation sequences are shown in fig. 4. At the bubble elongation stage at 0.1 m/s gas inlet velocity, the bubble appears to be smaller in size and the bubble neck elongates vertically due to the action of the buoyancy in comparison for other inlet velocities. This is different for 0.3 m/s and 0.2 m/s inlet velocities where the bubble neck elongates in a regular curvature (r_1) shape fashion. The bubble neck is about to break-off (or pinch-off stage) at $t = 0.19$ s, 0.11 s, 0.09 s of simulation time for 0.1, 0.2, and 0.3 m/s, respectively. A longer time is required for a lower inlet gas velocity and a significant effect is found for these inlet gas velocities when the bubble instantaneous contact angle (θ) had developed. The development of the θ with time in fig. 5 clearly identify the three stages of the bubble growth.

At the bubble growing stage, the buoyancy force increases and strongly acts on the whole bubble volume until the θ reaches a minimum value. This minimum θ has maintained until the end of bubble expansion stage. After passing the bubble expansion stage, the buoyancy force strongly acts on the upper portion of the bubble dome to form a bubble neck near the orifice (see fig. 4(a) to 4(c) at $t = 0.09$ s, 0.11 s, and 0.19 s, respectively). As the neck forms, the θ increases to form an obtuse angle. Eventually, the bubble pinches off and moves upward. For example: at $U_g = 0.1$ m/s, the θ is 55° on average and the period of minimum contact angle about 0.08 s but both the θ and the period of minimum contact angle decreased significantly to about 38° and 0.02 s, respectively, at $U_g = 0.3$ m/s. Therefore, it can be predicted that the minimum contact angle and period of the minimum flat angle decreases with higher gas velocity.

Generally, the gas pressure inside the bubble and the dynamic pressure depend on the bubble volume. The dynamic pressure mainly acts on the bubble dome surface and the maxi-

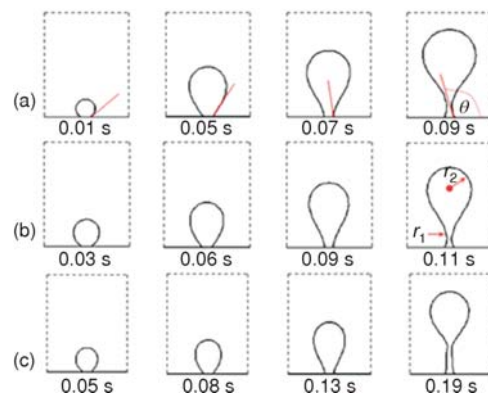


Figure 4. Contour image of bubble formation through 1 mm orifice of (a) 0.3 m/s, (b) 0.2 m/s, and (c) 0.1 m/s. Noted: θ , r_2 , and r_1 represent as contact angle, bubble dome, and bubble neck radius, respectively

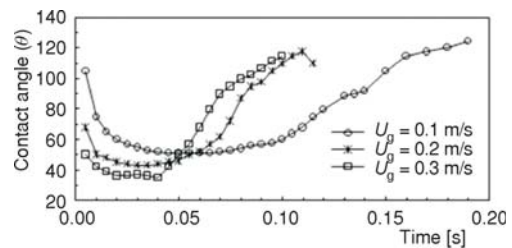


Figure 5. Instantaneous contact angle histories with time for the different inlet gas velocity

imum dynamic pressure depends on bubble volume (bubble shape), that can be explain with the Young-Laplace equation of $\Delta P = \sigma(1/r_0 + 1/r_2)$; where ΔP , $1/r_0$, and $1/r_2$ denotes as the pressure difference across the bubble surface, the orifice radius, and the bubble curvature radius, respectively. From the Young-Laplace equation, the maximum value of the pressure corresponds with the minimum radius. This statement had validated when the bubbles are in hemispherical shape that means the bubble curvature radius is equal to the orifice radius. Figure 6(a) and 6(b) show the development of differential of dynamic pressure on the bubble dome with the time during the expansion until the bubble shape becomes spherical. Results from fig. 6(a) have shown that the differential dynamic pressure increases steeply for high inlet gas velocity compared to low inlet gas velocity. For example: at $U_g = 0.3$ m/s, the maximum pressure ratio is found after a short time of 0.0001 s compared to 0.0022 s for the low inlet velocity of 0.1 m/s. The differential pressure on the bubble dome decreased monotonically after the bubble hemispherical shape until the bubble departure as shown in fig. 6(b). It can be found that the differential pressure decreases rapidly and need less time to increase again for high inlet gas velocity compared with the low inlet gas velocity.

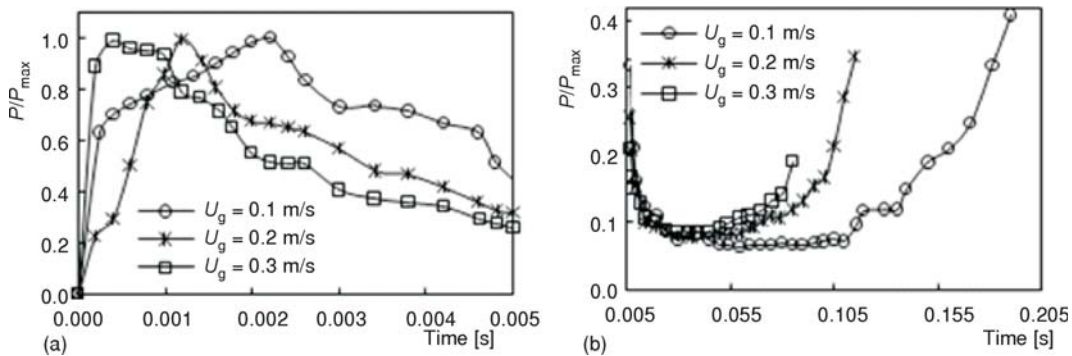


Figure 6. Differential of dynamic pressure on bubble dome with time; (a) before the bubble hemispherical shape and (b) after pass the hemispherical shape

For example, the gas velocity of 0.2 m/s and 0.3 m/s, the differential pressure shows an unsteady state because of the rapid change of dynamic pressure. But, for inlet velocity of 0.1 m/s, the differential pressure becomes steady for longer time ($t = 0.055$ - 0.105 s) at 0.08 of the maximum pressure. Thus, the faster bubble hemispherical shape forms for the high inlet gas velocity and stable dynamic pressure is found for the bubble of low inlet gas velocity.

The development of gas pressure inside the bubble due to the gas inlet velocity when the bubble becomes hemispherical and after pass the hemispherical shape is shown in fig. 7(a) and 7(b), respectively. It is found that the inside gas pressure increases with time until the bubble shape become hemispherical and gradually decreases after passing the bubble hemispherical shape. As shown in fig. 7(a), the highest pressure is found from the high inlet gas velocity and continue for a short period of time (0.3 m/s, 269.56 Pa, 0.0001 s) compared to low inlet gas velocity (0.1 m/s, 196.2 Pa, 0.0004 s). The gas pressure during expansion stage after passing the bubble hemispherical shape decreases gradually without remarkable effect of the inlet gas velocity, as shown in fig. 7(b).

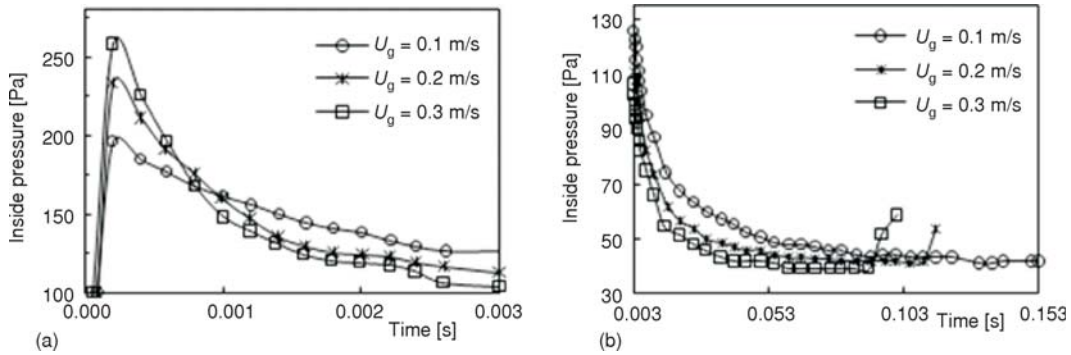


Figure 7. Gas pressure inside the bubble with time; (a) before the bubble hemispherical shape and (b) after pass the hemispherical shape

Figure 8 shows the departure diameter of the bubble as a function of inlet gas velocity. Note that, the bubble departure diameter is calculated using the inlet velocity, the orifice diameter and the time required for a bubble pinching off from the orifice. This is based on the formulation of $U_g A t_d = V_b = \pi d_c^3 / 6$ as suggested by Badam *et al.* [10] for bubble volume calculation. The bubble pinching time (or departure time), t_d is obtained from the CFD model.

In addition, we have compared the bubble departure diameter between the CFD and Bhavaraju *et al.* [25] correlation, as presented in fig. 8. The authors developed the correlations based on experimental study to determine the equivalent gas bubble diameter as function of the gas flow rate, the orifice diameter, the liquid density, the liquid viscosity and the surface tension. Bhavaraju *et al.* [25] correlation is given as:

$d_p = [3.23 d_o (\rho_l U_g d_o / \mu_l)^{-0.1} \times (U_g^2 \pi^2 / 16 g d_o)^{0.21}]$. It can be observed that the predicted simulation results increase with the increasing inlet gas velocity and quite consistent with the calculated correlation results. The relative error is less than 4.0% between the correlation results and simulation results.

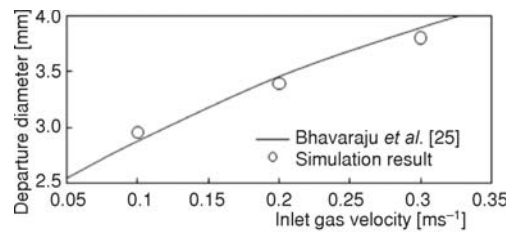


Figure 8. Variation of bubble departure diameter with inlet gas velocity at $d_o = 1$ mm; Bhavaraju *et al.* [25] correlation results also included

Effect of Reynolds number on bubble formation

The effect of Reynolds number (Re_μ) on the bubble formation dynamics through an orifice is investigated using cases 8 to 11. The Re_μ in the range of 1.58 to 120, which is tested, is varied using the liquid viscosity (tab. 1). Orifice diameter, $d_o = 1$ mm and the low inlet gas velocity, $U_g = 0.1$ m/s is used. Figure 9(a)-(d) shows the velocity field near the bubble neck before pinch off for cases 8-11, respectively. Generally, the buoyancy is one key force for the growth of a bubble. When the upper portion of the bubble becomes large enough; the bubble gradually is elongated more. The buoyancy force tends to lift the upper portion of the bubble whilst the bubble foot remains fixed to the orifice, and as result forming a neck near the bubble base. Further on, when the bubble grows due to the inlet gas velocity, a liquid circulation around the bubble neck pushes continuously. As a result, the elongated bubble neck alters to slender shape, which

is observed in the cases 8-11, fig. 9(a)-(d), respectively. For low Re_μ , fig. 9(a), larger elongation of the bubble neck is observed due to low pressure near the neck region. The low pressure region developed due to stronger push of liquid jet with a longer period, which tends to decrease progressively for the higher Re_μ due to weaker push of liquid jet that allows forming a strong liquid vortex near the neck region, fig. 9(b)-(d).

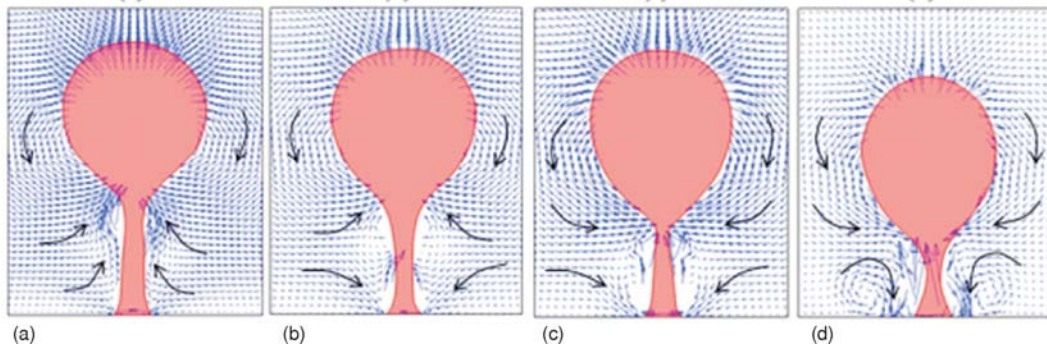


Figure 9. Velocity field around the bubble neck at $Bo_b = 0.187$; (a) $Re_\mu = 1.58$, $t = 0.19s$ (case-8), (b) $Re_\mu = 2.41$, $t = 0.175s$ (case-9), (c) $Re_\mu = 4.82$, $t = 0.162s$ (case-10), and (d) $Re_\mu = 120$, $t = 0.14s$ (case-11)

Additionally, a low Re_μ (high liquid viscosity), the bubble pinch off time delayed longer than the bubble with the higher Re_μ (low liquid viscosity) due to the development of weak liquid vortex around the bubble's slender neck. But the higher Re_μ of 120 (case-11) takes less time for the bubble pinch off due to stronger vortex ring, which developed near the orifice, resulting in earlier bubble pinch off with less elongation of the bubble neck, fig. 9(d) at $t = 0.14s$. On the other hand, the viscous force is always trying to maintain fluid motion with a minimum resistance. As a result, weaker stretching developed over the bubble surface for the Re_μ of 120 (case-11). These effects cause earlier pinch off for the higher Re_μ of bubble. Figure 10(a) compares the pinch-off time vs. Re_μ for cases 8-11 and cases 12-15. Note that, the density of the liquid in cases 12-15 is reduced to be the same as that of water. This result in a reduction of about 17% in Re_μ and Bo_b of that of cases 8-11. The bubble pinch off for cases 8-11 delayed (by 20%) when compared to that of cases 12-15.

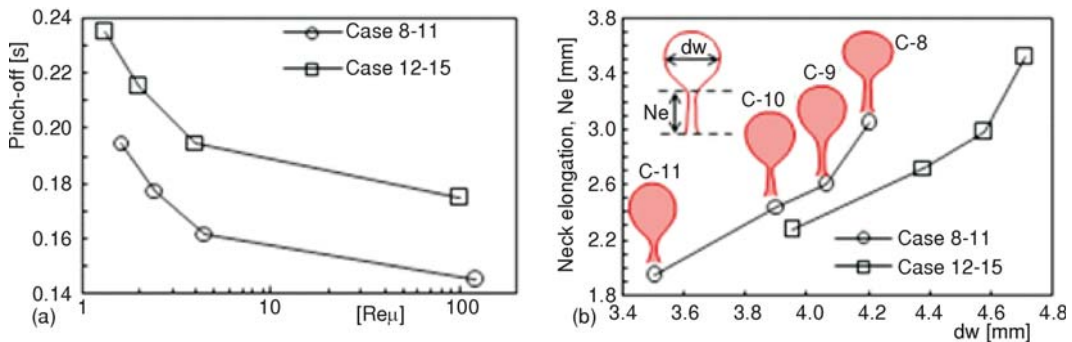


Figure 10. (a) Bubble pinch-off time as a function of Reynolds number, (b) bubble neck elongation as a function of bubble width

Figure 10(b) shows the bubble neck elongation (Ne) as a function of bubble width (dw) at different Reynolds number. It is observed that the bubble neck elongation decreases with decreasing of the bubble width. As compares between the cases 8-11 and cases 12-15 in fig. 10(b), it is found that the bubble elongation height and bubble width decrease around 15% and 13%, respectively, when compared to that of cases 12-15. Thus, the reduction of the Re_μ and Bo_b by about 17% suggesting water assists the bubble formation from an orifice.

Conclusions

In this paper, the VOF-CSF method have been used to investigate the effect of inlet gas velocity from 0.1 m/s to 0.3 m/s through an orifice diameter of 1 mm and the effect of Reynolds number on bubble formation in viscous liquid. The detailed information of bubble formation on various stages is presented using the CFD model. The study has demonstrated the capability of CFD to predict the bubble velocity, bubble shape, and departure diameter with a good accuracy compared to experimental data. The conclusions of the study are:

- at the bubble formation stage, the faster changes of bubble contact angle from an obtuse angle to an acute angle were found for the higher inlet gas velocity,
- larger size of bubble formed at the higher inlet gas velocity which maintained low static pressure and required less time to form the bubble hemispherical shape,
- an increase of Reynolds number from 1.58 to 120 sped up the bubble pinch-off and formed a smaller bubble neck height due to stronger vortex ring around the bubble neck, and
- reducing Reynolds number and Bond number of 17% required quit longer period (by roughly 20%) to the bubble pinch-off as well as the height of the bubble necks and the bubble width reduced around 15% and 13%, respectively.

Acknowledgments

This research is financially supported by University of Malaya, Ministry of Higher Education High Impact Research (UM.C/HIR/MOHE/ENG/13), and University of Malaya Research Grant (UMRG: RG121/11AET).

Nomenclature

A	– orifice area, [m ²]
Bo_b	– Bond number ($=\Delta\rho g d_o^2/\sigma$), [-]
d_e	– equivalent diameter, [mm]
d_o	– orifice diameter, [mm]
d_p	– departure diameter, [mm]
\vec{F}	– external forces, [N]
g	– gravitational acceleration, [ms ⁻²]
H	– bubble height, [mm]
T	– tensor, [Nm ⁻²]
t	– time, [s]
t_d	– detachment time, [s]
P	– pressure, [Nm ⁻²]
Re_μ	– orifice Reynolds number ($\rho_1 U_g d_o/\mu_1$), [-]

U_g	– inlet gas velocity, [ms ⁻¹]
U_T	– bubble terminal velocity, [ms ⁻¹]
\vec{V}	– velocity vector, [ms ⁻¹]
V_b	– bubble volume, [m ³]
W	– bubble width, [mm]

Greek symbols

α_g	– volume fraction of liquid phase, [-]
α_l	– volume fraction of liquid phase, [-]
m_1	– viscosity of fluid, [Pa·s]
ρ_1	– density of fluid, [kgm ⁻³]
σ	– surface tension coefficient, [Nm ⁻¹]

References

- [1] Ku, X. K., *et al.*, Eulerian-Lagrangian Simulation of a Bubbling Fluidized Bed Reactor: Assessment of Drag Force Correlations, *Thermal Science*, 16 (2012), 5, pp. 1442-1445
- [2] Mladenović, M. R., *et al.*, Numerical Simulation of Non-Conventional Liquid Fuels Feeding in a Bubbling Fluidized Bed Combustor, *Thermal Science*, 17 (2013), 4, pp. 1163-1179

- [3] Kulkarni, A. A., Joshi, J. B., Bubble Formation and Bubble Rise Velocity in Gas-Liquid Systems: A Review, *Industrial & Engineering Chemistry Research*, 44 (2005), 16, pp. 5873-931
- [4] Canneto, G., et al., Numerical Simulation of Gas-Solid Flow in an Interconnected Fluidized Bed, *Thermal Science*, 19 (2015), 1, pp. 317-328
- [5] Davidson, J., Schuler, B., Bubble Formation at an Orifice in a Viscous Liquid, *Chemical Engineering Research and Design*, 75 (1997), Suppl., pp. S105-S115
- [6] Zhang, L., Shoji, M., Aperiodic Bubble Formation from a Submerged Orifice, *Chemical Engineering Science*, 56 (2001), 18, pp. 5371-81
- [7] Tsuge, H., et al., Bubble Formation Mechanism from Downward Nozzle-Effect of Nozzle Shape and Operating Parameters, *Chemical Engineering Science*, 61 (2006), 10, pp. 3290-3298
- [8] Hamad, F. A., et al., Comparison of Experimental Results and Numerical Predictions of Drop Diameter from a Single Submerged Nozzle in a Liquid-Liquid System, *Canadian Journal of Chemical Engineering*, 79 (2001), 3, pp. 322-328
- [9] Di Bari, S., et al., A Numerical Study of Quasi-Static Gas Injected Bubble Growth: Some Aspects of Gravity, *International Journal of Heat and Mass Transfer*, 64 (2013), Sept., pp. 468-482
- [10] Badam, V., et al., Experimental Investigations of Regimes of Bubble Formation on Submerged Orifices Under Constant Flow Condition, *Canadian Journal of Chemical Engineering*, 85 (2007), 3, pp. 257-267
- [11] Valencia, A., et al., Numerical Simulation of Gas Bubbles Formation at a Submerged Orifice in a Liquid, *International Communications in Heat and Mass Transfer*, 29 (2002), 6, pp. 821-830
- [12] Gerlach, D., et al., Numerical Simulation of Periodic Bubble Formation at a Submerged Orifice with Constant Gas Flow Rate, *Chemical Engineering Science*, 62 (2007), 7, pp. 2109-2125
- [13] Chakraborty, I., et al., Computational Investigation on Bubble Detachment from Submerged Orifice in Quiescent Liquid under Normal and Reduced Gravity, *Physics of Fluids*, 21 (2009), 6, 062103
- [14] Brackbill, J., et al., A Continuum Method for Modeling Surface Tension, *Journal of Computational Physics*, 100 (1992), 2, pp. 335-354
- [15] Youngs, D., Time-Dependent Multi-Material Flow with Large Fluid Distortion, in: *Numerical Methods for Fluid Dynamics*, (Eds. K. W. Morton, M.J. Braines), Academic Press, New York, USA, 1982, pp. 273-285
- [16] Krishna, R., Van Baten, J., Rise Characteristics of Gas Bubbles in a 2D Rectangular Column: VOF Simulations vs. Experiments, *International Communications in Heat and Mass Transfer*, 26 (1999), 7, pp. 965-974
- [17] Raymond, F., Rosant, J. -M., A Numerical and Experimental Study of the Terminal Velocity and Shape of Bubbles in Viscous Liquids, *Chemical Engineering Science*, 55 (2000), 5, pp. 943-955
- [18] Hirt, C.W., Nichols, B. D., Volume of Fluid (VOF) Method for the Dynamics of Free Boundaries, *Journal of Computational Physics*, 39 (1981), 1, pp. 201-225
- [19] ***, Fluent, I., FLUENT 6.3 User's Guide, Fluent Documentation, 2006
- [20] Ma, D., et al., Two-Dimensional Volume of Fluid Simulation Studies on Single Bubble Formation and Dynamics in Bubble Columns, *Chemical Engineering Science*, 72 (2012), Apr., pp. 61-77
- [21] Kulkarni, A., et al., On the Development of Flow Pattern in a Bubble Column Reactor: Experiments and CFD, *Chemical Engineering Science*, 62 (2007), 4, pp. 1049-1072
- [22] Kantarci, N., et al., Bubble Column Reactors, *Process Biochemistry*, 40 (2005), 7, pp. 2263-2283
- [23] Krishna, R., et al., Wall Effects on the Rise of Single Gas Bubbles in Liquids, *International Communications in Heat and Mass Transfer*, 26 (1999), 6, pp. 781-790
- [24] Kim, I., et al., Modeling Bubble and Drop Formation in Flowing Liquids in Microgravity, *AIChE Journal*, 40 (1994), 1, pp. 19-28
- [25] Bhavaraju, S., et al., Bubble Motion and Mass Transfer in Non-Newtonian Fluids: Part I. Single Bubble in Power Law and Bingham Fluids, *AIChE Journal*, 24 (1978), 6, pp. 1063-1070